ACS APPLIED MATERIALS & INTERFACES

www.acsami.org Research Article

Three-Dimensional Surface Treatment of MoS_2 Using BCl_3 Plasma-Derived Radicals

Heesoo Lee,[§] Hoijoon Kim,[§] Kihyun Kim,[§] Kwangsik Jeong, Mirine Leem, Seunghyun Park, Jieun Kang, Geunyoung Yeom,* and Hyoungsub Kim*

Cite This: ACS Appl. Mater. Interfaces 2023, 15, 46513−46519 Read Online

ACCESS | Metrics & More | Article Recommendations | Supporting Information

Downloaded via SUNGKYUNKWAN UNIV on November 9, 2023 at 06:52:54 (UTC).
See https://pubs.acs.org/sharingguidelines for options on how to legitimately share published articles.

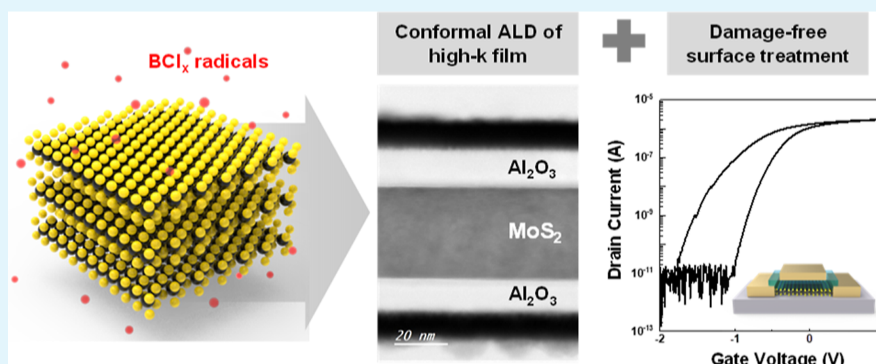

ABSTRACT: The realization of next-generation gate-all-around field-effect transistors (FETs) using two-dimensional transition metal dichalcogenide (TMDC) semiconductors necessitates the exploration of a three-dimensional (3D) and damage-free surface treatment method to achieve uniform atomic layer-deposition (ALD) of a high-k dielectric film on the inert surface of a TMDC channel. This study developed a BCl_3 plasma-derived radical treatment for MoS_2 to functionalize MoS_2 surfaces for the subsequent ALD of an ultrathin Al_2O_3 film. Microstructural verification demonstrated a complete coverage of an approximately 2 nm-thick Al_2O_3 film on a planar MoS_2 surface, and the applicability of the technique to 3D structures was confirmed using a suspended MoS_2 channel floating from the substrate. Density functional theory calculations supported by optical emission spectroscopy and X-ray photoelectron spectroscopy measurements revealed that BCl radicals, predominantly generated by the BCl_3 plasma, adsorbed on MoS_2 and facilitated the uniform nucleation of ultrathin ALD−Al_2O_3 films. Raman and photoluminescence measurements of monolayer MoS_2 and electrical measurements of a bottom-gated FET confirmed negligible damage caused by the BCl_3 plasma-derived radical treatment. Finally, the successful operation of a top-gated FET with an ultrathin ALD−Al_2O_3 (~5 nm) gate dielectric film was demonstrated, indicating the effectiveness of the pretreatment.

KEYWORDS: *MoS_2, surface functionalization, BCl_3 plasma, radicals, atomic layer deposition, high-k dielectric*

1. INTRODUCTION

For a continuous technical node scaling of Si field-effect transistors (FETs), gate-all-around FETs (GAAFETs) with multiple nanosheet- or nanowire-shaped channels completely wrapped with a high-k gate dielectric film are projected to gradually replace FETs with fin structures.[1,2] Moreover, ultrathin Si channels in GAAFETs are expected to be replaced with alternative semiconductors in the future, such as transition metal dichalcogenides (TMDCs) with two-dimensional (2D) layer structures, which are more immune to mobility degradation and short-channel effects than Si, even at subnanometer thicknesses.[3,4] Thus, to ensure uniform encapsulation of TMDC channel layers within a three-dimensional (3D) GAAFET structure, it is essential to employ an atomic layer deposition (ALD) process that allows the deposition of an ultrathin high-k gate dielectric film with excellent step coverage capabilities and electrical properties.[5,6] However, the absence of chemically reactive bonds on TMDC surfaces hinders the uniform growth of ultrathin high-k gate dielectric films during ALD at high temperatures, necessitating the development of various surface treatments and passivation techniques.[7] In addition, to implement a GAAFET with multiple TMDC channels, it is necessary to develop a damage-free 3D surface-treatment method.

Received: June 28, 2023
Accepted: September 8, 2023
Published: September 20, 2023

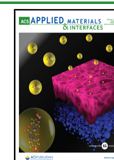

 © 2023 American Chemical Society

https://doi.org/10.1021/acsami.3c09311
ACS Appl. Mater. Interfaces 2023, 15, 46513−46519

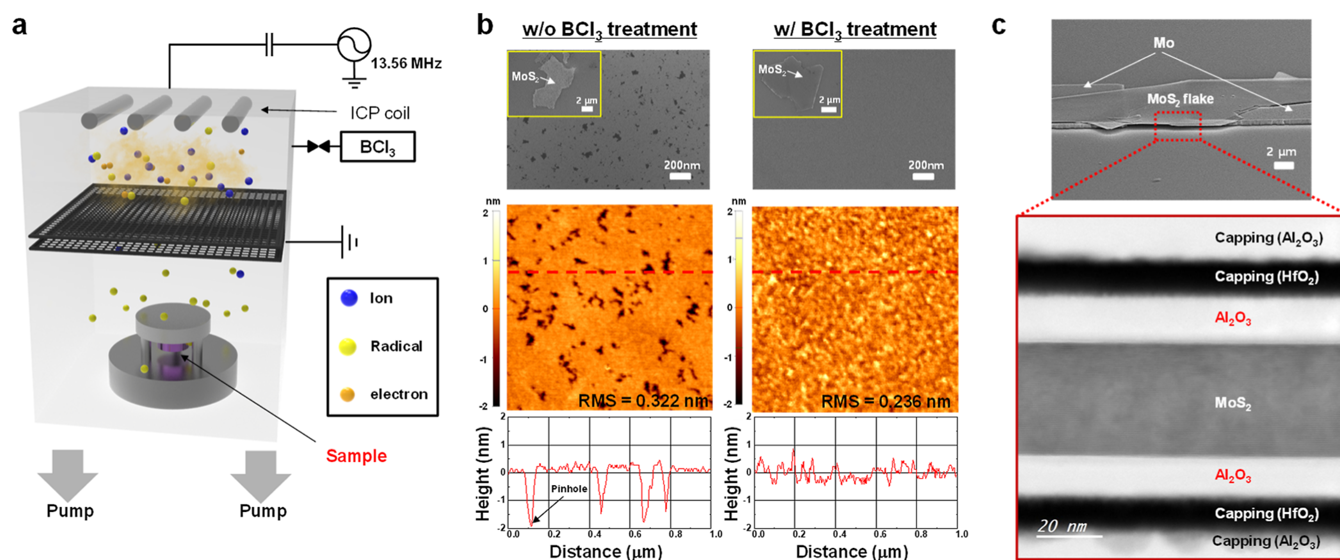

Figure 1. ALD coverage improvement by BCl_3 plasma-derived radical treatment and its applicability to a 3D structure. (a) Schematic of the remote plasma chamber used for BCl_3 plasma-derived radical treatment. (b) SEM (top) and AFM (middle and bottom) results of ALD−Al_2O_3 (~2 nm) on MoS_2 flakes with and without BCl_3 plasma-derived radical treatment. (c) TEM analysis results of the ALD of Al_2O_3 on the BCl_3 plasma-derived radical-treated MoS_2 flakes suspended by patterned Mo supports.

Although many approaches have been proposed to enhance the deposition uniformity and thickness scalability of high-k films on 2D TMDC surfaces,[7] little attention has been paid to addressing these issues on 3D TMDC substrates. One potential technique for the surface treatment of 3D structures is the use of chemically reactive and electrically neutral radicals generated in a plasma process, without directionality. Previous studies utilized O_2[8−10] and Cl_2[11] plasmas for the treatment of 2D TMDC surfaces. The O_2 plasma treatment significantly improved the coverage of subsequent ALD high-k films on MoS_2.[8,9] However, as a side effect, the simultaneous formation of Mo oxide may increase the off-current of FETs.[10] Although the Cl_2 plasma treatment improved the MoS_2 FET performance, it was only used to modify the MoS_2 channel surface in a bottom-gated FET configuration without subsequent deposition of high-k films.[11]

This study used a novel 3D and nondestructive treatment approach for MoS_2 surfaces that employs BCl_3 plasma-derived radicals to promote uniform nucleation of high-k gate dielectric films in subsequent ALD.[12] To demonstrate the 3D surface treatment capability of BCl_3-generated radicals, a remote plasma system with an ion-filtering mesh was utilized and the sample was placed upside down. The facile and uniform growth of an ultrathin Al_2O_3 film using ALD was demonstrated, which exhibited outstanding compatibility with 3D structures. Additionally, the working mechanism of this process was proposed based on density functional theory (DFT) calculations. Furthermore, the absence of physical damage during treatment was verified by fabricating and electrically characterizing the MoS_2 FETs with bottom- and top-gated structures.

2. EXPERIMENTAL DETAILS

2.1. BCl_3 Plasma-Derived Radical Treatment of MoS_2. A 13.56 MHz AC inductively coupled plasma (ICP) generator was used to generate the BCl_3 remote plasma. Figure 1a illustrates the custom-built remote ICP reactor used in this study, which underwent modifications involving the insertion of two electrically grounded mesh grids made of stainless steel with a thickness of 0.14 mm. These mesh grids were identical, featuring a square array of square holes measuring 0.135 × 0.135 mm. They were overlapped without twisting and were spaced approximately 2 cm apart. The primary purpose of this modification was to use the mesh grids as a plasma shield to prevent the ions produced by the plasma from reaching the substrate, effectively covering an area of 30 × 30 cm, consistent with the chamber dimensions. The use of two mesh grids aimed to enhance the prevention of ions more effectively. In addition, to indirectly demonstrate the potential applicability of the proposed process to 3D-structured devices such as GAAFETs, the specimens were attached to an inverted 4-inch Si wafer that was floated approximately 1.5 mm above the bottom of the plasma chamber. The optimal BCl_3 plasma parameters in our system, such as plasma power (250 W), working pressure (2.1 mTorr), and treatment time (300 s), were preselected by comparing the surface coverage of the ALD−Al_2O_3 thin films on the single crystalline MoS_2 flakes using plan-view scanning electron microscopy (SEM), as shown in Figure S1. As soon as the treatment was completed, the samples were loaded into the ALD chamber within 5 min to minimize their exposure to ambient air. The chemical species produced by BCl_3 plasma were analyzed through optical emission spectroscopy (OES, Isoplane SCT 3200) using a grating with a blaze wavelength of 300 nm and a groove density of 1200 mm^{-1}.

2.2. ALD of Al_2O_3 and Fabrication of MoS_2 FETs. Heavily p-type-doped Si substrates with thick SiO_2 films (90 nm) were cleaned with acetone and isopropyl alcohol (IPA) for 3 min each using a sonicator, and then thick MoS_2 flakes mechanically exfoliated from a bulk crystal (470MOS2M-AB, SPI Supplies) were transferred onto the substrates using conventional 3 M scotch tape. Any remaining tape residues on the MoS_2 flakes were removed by immersing the samples in acetone at 80 °C for 1 h, followed by rinsing with IPA. The ALD of Al_2O_3 was conducted at a process pressure of ~0.1 Torr in a laboratory-scale and custom-built thermal ALD system with a traveling wave design, using trimethylaluminum (TMA) and H_2O precursors. Because lower temperatures are known to improve film coverage on MoS_2 by suppressing the thermal desorption of precursors,[13] the lowest deposition temperature of 200 °C was selected while remaining within the typical Al_2O_3 ALD window of 200−300 °C.[14] Each ALD cycle consisted of a series of injections of TMA (1 s), N_2 (20 s), H_2O (5 s), and N_2 (30 s). The TMA and H_2O canisters were maintained at a temperature of 9 °C, and their delivery lines were heated to 60 and 100 °C, respectively. The thickness of the Al_2O_3 films was monitored on dummy Si substrates cleaned with a 1%

https://doi.org/10.1021/acsami.3c09311
ACS Appl. Mater. Interfaces 2023, 15, 46513−46519

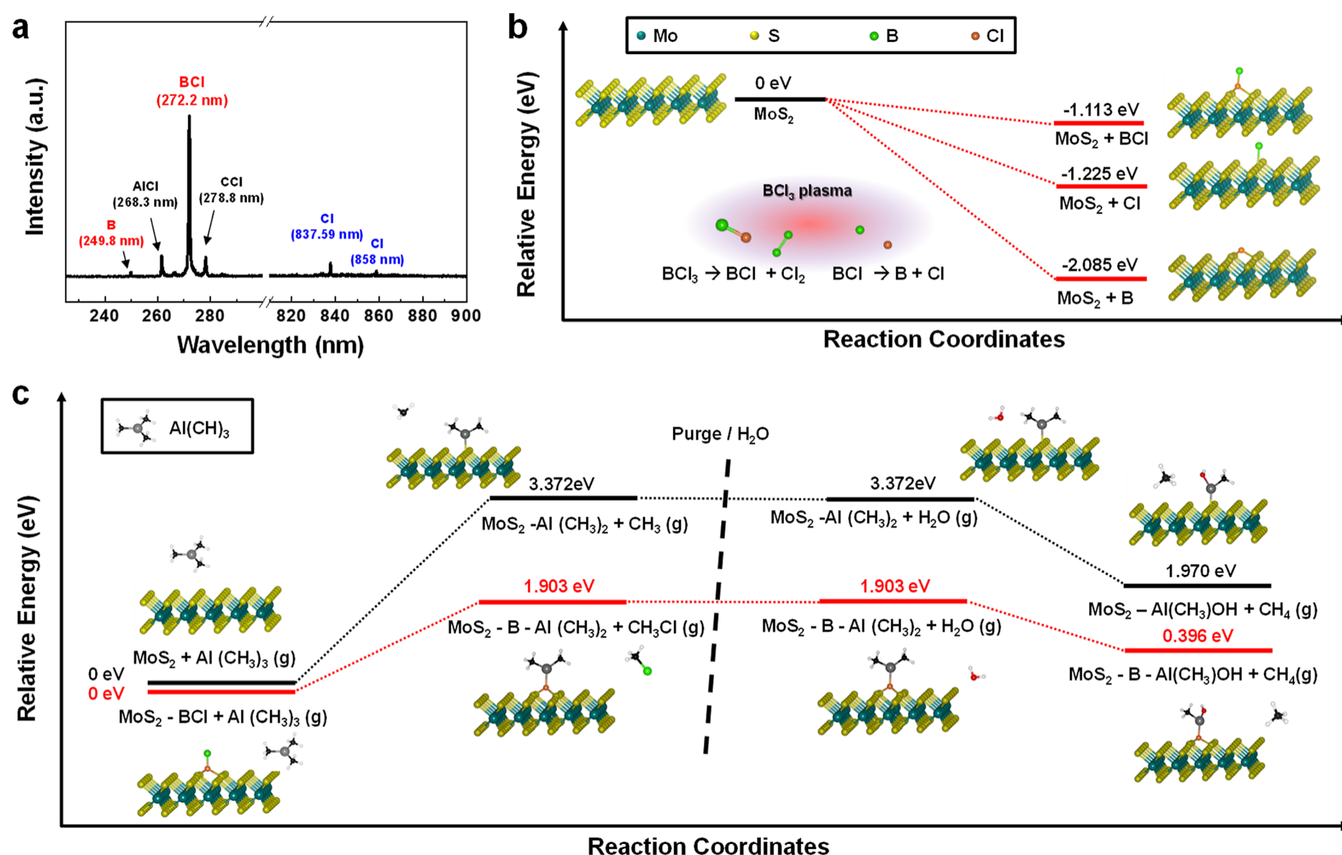

Figure 2. Mechanism analyses for the BCl_3 plasma-derived radical treatment and the subsequent Al_2O_3 ALD process. (a) OES analysis result of BCl_3 plasma. (b) DFT modeling of the adsorption energy reaction pathways of BCl_3 plasma-generated radicals on the MoS_2 surface. (c) Comparison of the energy reaction pathways of the ALD−Al_2O_3 deposition process on MoS_2 surfaces with and without adsorbed BCl radicals, based on DFT modeling.

HF solution, which was subjected to a simultaneous ALD process with the MoS_2 substrates. Thickness measurements were conducted using a spectroscopic ellipsometer (SE MG-1000UZ, NANO-VIEW) at the MEMS Sensor Platform Center of Sungkyunkwan University. The deposition rate of the Al_2O_3 film on Si was approximately 1 Å/cycle at 200 °C.

To fabricate both bottom- and top-gated MoS_2 FETs, a Cr/Au source/drain layer with a thickness of 10 nm/50 nm was deposited using e-beam evaporation followed by a lift-off patterning process. An identical Cr/Au layer was used for the top-gate electrode in a top-gated MoS_2 FET after the deposition of the Al_2O_3 top-gate dielectric on MoS_2 pretreated with BCl_3 plasma-derived radicals.

2.3. Characterization Methods and DFT Calculations. The surface coverage of the ALD−Al_2O_3 films on MoS_2 was examined using SEM (S-4700, Hitachi). In addition, cross-sectional transmission electron microscopy (TEM, ARM 200F, JEOL) was used to observe the conformal deposition characteristics of ALD−Al_2O_3 on MoS_2 flakes pretreated with BCl_3 plasma-derived radicals. The TEM samples were prepared using a focused ion beam (SMI 3050TB, SII NanoTechnology Inc.) system. The possible changes of chemical bonds on the MoS_2 surface during the BCl_3 plasma-derived radical treatment and/or ALD−Al_2O_3 were examined using X-ray photoelectron spectroscopy (XPS, MultiLab 2000, Thermo VG) with an Mg Kα source. A Raman and photoluminescence (PL) spectrometer (Alpha 300M+, Witec) was used to identify and characterize the monolayer MoS_2 flakes transferred onto SiO_2 to evaluate the BCl_3 plasma-derived radical treatment effect. The electrical properties of the fabricated MoS_2 FETs were characterized using a Keysight B1500A semiconductor parameter analyzer.

To examine the energy changes during the chemical process and the effects of the BCl_3 plasma-derived radical treatment, DFT calculations were performed using a Vienna ab initio simulation package (VASP) with a PBEsol functional.[15−17] The first step involved geometric optimization of the MoS_2 unit cell, which was performed until a convergence condition of 0.01 eV/Å was satisfied using 11 × 11 × 3 *k*-points for a *k*-spacing of <0.2/Å and a cutoff energy of 500 eV. To calculate the formation energy of the MoS_2−molecular chemical bonds that could be generated during the ALD process, a 5 × 5 supercell with one layer of MoS_2 structure was generated from the optimized unit cell. Γ (gamma) *k*-points and 3 × 3 × 1 *k*-points were used for geometry optimization and formation energy calculations. Based on the difference in the formation energy between the reactant and product, we evaluated the ALD reaction pathway that synthesized Al_2O_3 on MoS_2 with TMA and H_2O.

3. RESULTS AND DISCUSSION

3.1. Coverage Improvement and Applicability to 3D Structures. First, the improvement in the ALD−Al_2O_3 film coverage on MoS_2 through BCl_3 plasma-derived radical treatment was demonstrated, as shown in Figure 1b. The Al_2O_3 films were deposited on both BCl_3 plasma-treated and untreated thick MoS_2 flakes for 20 ALD cycles, resulting in the formation of approximately 2 nm-thick Al_2O_3 films on Si at 200 °C. Subsequently, the surface coverage of the films was examined using SEM and AFM. On the pristine surface of MoS_2 without any treatment, ALD led to the formation of Al_2O_3 islands with numerous pinholes, indicating incomplete coverage, as observed using SEM and AFM. This phenomenon can be attributed to the higher degree of physical adsorption of the ALD precursors rather than their chemical bonding with MoS_2, as reported previously.[7] In contrast, after the BCl_3 plasma-derived radical treatment, the formation of a

https://doi.org/10.1021/acsami.3c09311
ACS Appl. Mater. Interfaces 2023, 15, 46513−46519

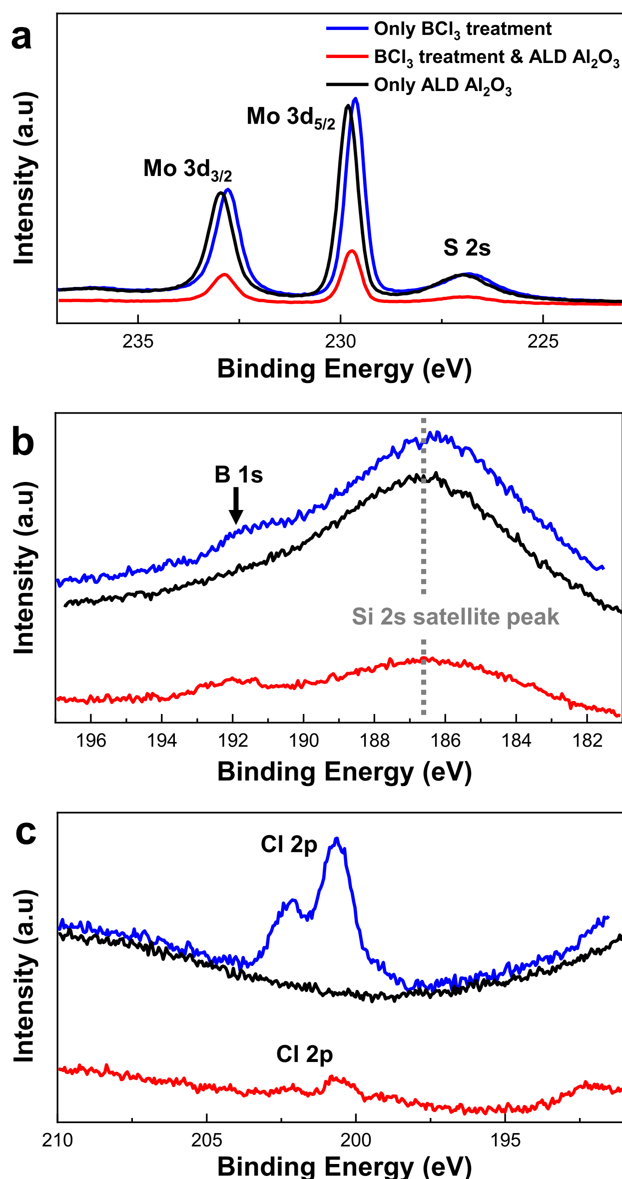

Figure 3. Results of the chemical analysis after various surface passivation. (a) Mo 3d and S 2s, (b) B 1s, and (c) Cl 2p XPS peaks observed in the MoS_2 flakes that underwent different surface passivation: only BCl_3 plasma-derived radical treatment (blue line), BCl_3 plasma-derived radical treatment followed by ALD of Al_2O_3 (red line), and only ALD of Al_2O_3 (black line).

continuous Al_2O_3 thin film was identified, as confirmed by the corresponding SEM and AFM images (Figure 1b), which exhibited conformal deposition without any detectable pin-holes.

The hardware configuration of the BCl_3 plasma-derived radical treatment system was specifically designed to expose the MoS_2 surface to radical species with minimal directionality (Figure 1a). This feature enables the application of BCl_3 plasma-derived radical treatment to 3D sample structures, facilitating the conformal wrapping of a 2D sheet channel with a high-k dielectric film, which is necessary for GAAFET design. To demonstrate the potential applicability of the BCl_3 plasma-derived radical treatment to a 3D-structured device, a MoS_2 bridge structure resembling an actual GAAFET device was fabricated, as shown in Figure 1c. The bridge structure was designed to suspend the thick MoS_2 flakes above the SiO_2 substrate using two separate Mo (thickness of ∼500 nm) supports. These supports were sputter-deposited and patterned using photolithography and etching with a conventional wet etchant (Mo-72, purchased from WINCHEM Co.); the detailed steps of the fabrication are illustrated in Figure S2. After the BCl_3 plasma-derived radical treatment and ALD−Al_2O_3 film deposition (target thickness of ∼12 nm on Si) on the fabricated bridge structure, a cross-sectional TEM sample was prepared and analyzed, as shown in Figure 1c. To provide structural stabilization for the suspended MoS_2 flake during TEM sampling, an additional layer of the ALD−Al_2O_3 film with a thickness of approximately 200 nm was deposited to fill the gap between the MoS_2 and the substrate. In addition, to differentiate the two Al_2O_3 layers, an approximately 10 nm-thick ALD−HfO_2 film was inserted between them. Figure 1c shows the conformal deposition of an ALD−Al_2O_3 film, although a slightly thinner layer was deposited on the bottom side of the MoS_2 flakes, possibly due to an insufficient supply of ALD precursors.

3.2. Theoretical Mechanism Analyses. DFT calculations were conducted to investigate the mechanism by which the BCl_3 plasma-derived radical treatment enhanced ALD deposition on MoS_2. Our models included the adsorption of plasma-generated radicals and ALD precursors, while the atmospheric adsorbates generated during the ex situ process were not taken into consideration. The stable pathway for these reactions was determined by comparing the molecular formation energies before and after the reaction. Before DFT modeling of the plasma process was performed, an OES tool was used to experimentally examine the chemical species produced by the BCl_3 plasma. The spectra of the OES in Figure 2a confirm the generation of a small amount of B and Cl radicals as well as a dominant amount of BCl radicals within the plasma. A small peak corresponding to AlCl observed in the OES spectrum was likely a result of the chemical reaction between BCl_3 and the Al chamber wall. To check the possibility of enhanced nucleation of Al_2O_3 on MoS_2 through the production of AlCl during BCl_3 plasma pretreatment, a separate experiment was conducted using a similarly configured BCl_3 plasma system with an Al-free chamber. The results showed a similar improvement in the coverage of Al_2O_3 on MoS_2, suggesting that the coverage improvement observed in the main experiment was mostly induced by the presence of B, Cl, and BCl radicals rather than by the influence of the Al chamber wall.

The DFT calculation results shown in Figure 2b indicate that the energy reaction of the produced B, Cl, and BCl radicals enabled their stable adsorption onto the MoS_2 surface. This adsorption served as a mediator, facilitating the binding of the metal precursor during the subsequent ALD process. Consequently, the adsorption of TMA molecules onto the preadsorbed B, Cl, and BCl radicals on the MoS_2 surface was found to be a more energetically stable reaction pathway than direct adsorption on the MoS_2 surface. For instance, when the BCl radicals, identified as the predominant species in the plasma according to OES analysis, were preadsorbed on MoS_2 followed by the ALD−Al_2O_3 deposition process (Figure 2c), the Cl atoms readily transitioned to a gaseous state because of their strong binding to the CH_3 groups of TMA. Consequently, stable MoS_2−B−$Al(CH_3)_2$ bonds were formed as the final products on the MoS_2 surface. Therefore, the ALD pathway with BCl radical treatment was more energetically favorable than direct ALD deposition, and the energy of the

https://doi.org/10.1021/acsami.3c09311
ACS Appl. Mater. Interfaces 2023, 15, 46513−46519

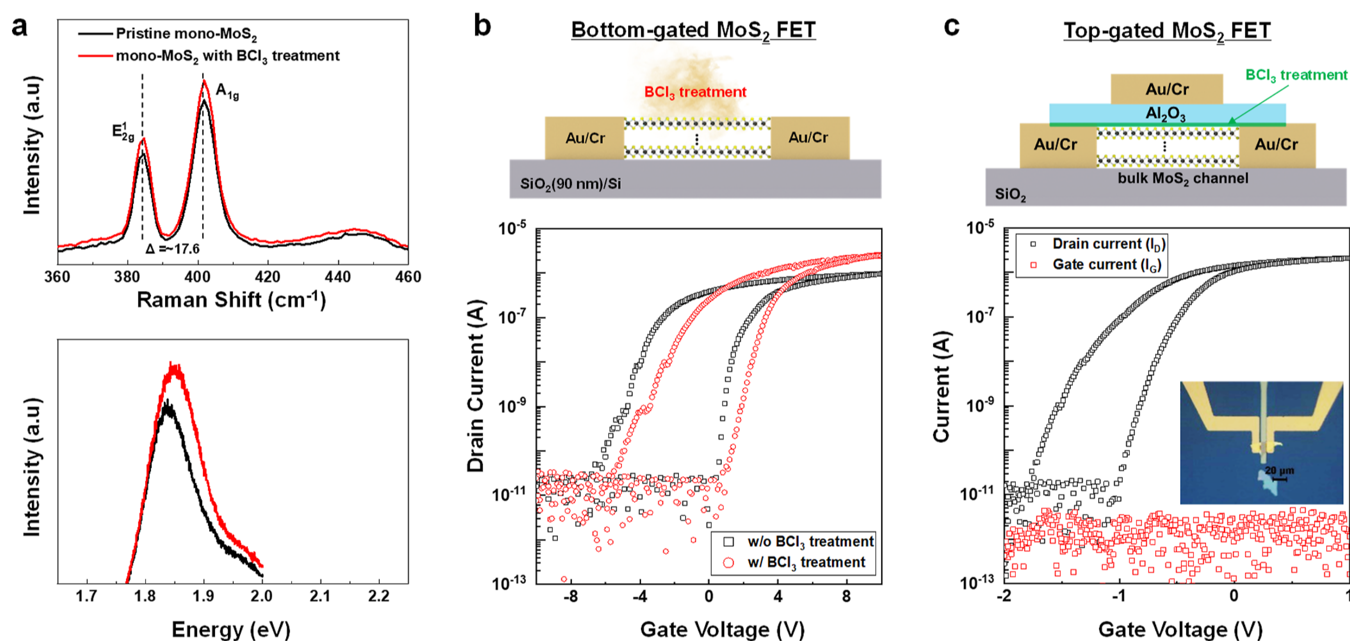

Figure 4. Electrical characteristics after BCl_3 plasma-derived radical treatment. (a) Raman and PL spectra of a monolayer MoS_2 flake with and without BCl_3 plasma-derived radical treatment. (b) Schematic (top) and transfer curve (bottom) of a bottom-gated bulk MoS_2 FET (channel length and width of 10 μm each) before and after BCl_3 plasma-derived radical treatment. (c) Schematic (top) and transfer curve (bottom) of a top-gated bulk MoS_2 FET with BCl_3 plasma-derived radical treatment followed by ALD of Al_2O_3 (~5 nm) as the top gate dielectric. Inset in panel (c) is an optical image of a fabricated top-gated bulk MoS_2 FET (channel length and width of 10 and 15 μm, respectively).

final state of MoS_2−B−$Al(CH_3)_2$ was approximately 80% lower than that of MoS_2−$Al(CH_3)_2$ in the ALD process without any pretreatment.

To validate the aforementioned DFT calculation model experimentally, XPS measurements were conducted on thick MoS_2 flakes coated with an ALD−Al_2O_3 (~2 nm) film, both with and without BCl_3 plasma pretreatment, as shown in Figure 3. The C 1s peak with a binding energy of 284.8 eV was used as the calibration reference for all the measured XPS spectra.[18] In the pretreated MoS_2 samples before and after Al_2O_3 deposition, B 1s (~192 eV) and Cl 2p (~201 and ~200 eV for $2p_{1/2}$ and $2p_{3/2}$ peaks, respectively) peaks were observed. These observations confirmed the facile chemical adsorption of B, Cl, and BCl radicals on MoS_2, consistent with the results of the DFT calculations. Notably, the intensity of the Mo peak was significantly reduced following the deposition of Al_2O_3 on the MoS_2 surface pretreated with the BCl_3 plasma-derived radicals because of the Al_2O_3 thickness effect, whereas a negligible change in the Mo peak intensity was observed for the untreated sample. This finding again confirms that the BCl_3 plasma-derived radical treatment enhanced the nucleation of Al_2O_3 and led to enhanced coverage on the MoS_2 surface.

3.3. Possible Physical Damage and FET Performance.

As discussed in the experimental section, the hardware configuration for the BCl_3 plasma-derived radical treatment was carefully optimized to minimize physical damage to the MoS_2 surface by removing the ionic species produced by the BCl_3 plasma. To directly assess the possible adverse effects of the treatment on the MoS_2 surface, a monolayer MoS_2 flake prepared using the gold exfoliation method[19] was used for Raman and PL measurements, as shown in Figure 4a. In the Raman spectrum, distinctive peaks associated with MoS_2, including the in-plane mode (E_{2g}) and the out-of-plane mode (A_{1g}), were observed at ~384.1 and ~401.7 cm^{-1}, respectively, when using a 532 nm excitation laser wavelength. The distance between these two peaks (~17.6 cm^{-1}) was used to experimentally confirm the MoS_2 monolayer following a reference source.[20] Compared with the pristine state, the Raman peak positions of MoS_2 remained nearly unchanged, and no decrease in their intensity was observed, even after treatment with a monolayer of MoS_2. These observations strongly indicate that the MoS_2 flakes were not noticeably etched during BCl_3 plasma-derived radical treatment. In the corresponding PL spectra of the monolayer MoS_2 flakes before and after treatment, no evidence of etching or degradation of MoS_2 was observed, as there were no significant changes, except for a slight increase in the intensity of the main peak. This change in the main PL peak is consistent with previous research on the chemical doping of MoS_2,[21] suggesting that radicals adsorbed on MoS_2 may induce subtle doping effects.

To further confirm the minimal adverse effects of the BCl_3 plasma-derived radical treatment on MoS_2, bottom-gated FETs were fabricated using a thick bulk MoS_2 flake (tens of nanometers) and a SiO_2 gate dielectric (90 nm). The drain current−gate voltage (I_D−V_G) characteristics were measured at a fixed drain voltage of 0.1 V, as shown in Figure 4b. There was no increase in the off-current level of the bottom-gated FET after the BCl_3 plasma-derived radical treatment, indicating that there was no detectable damage on the MoS_2 channel. However, a noticeable shift in the I_D−V_G curve toward a positive gate voltage was observed after surface treatment. This shift can be attributed to the doping effect caused by the binding of B to MoS_2, which is consistent with that observed in the PL spectra (Figure 4a). Furthermore, the increase in the on-current level of the device with the surface treatment could be attributed to the removal of absorbed OH species on the channel, which degraded the electrical properties of the device,[22] because of the BCl_3 plasma-generated radicals.

To demonstrate the potential application of the BCl_3 plasma-derived radical treatment on MoS_2 for subsequent

https://doi.org/10.1021/acsami.3c09311
ACS Appl. Mater. Interfaces 2023, 15, 46513−46519

ALD of high-k films, top-gated FETs were fabricated using a bulk MoS_2 flake and an ultrathin Al_2O_3 gate dielectric (target thickness of approximately 5 nm on Si). The resulting device structure and representative I_D-V_G characteristics are shown in Figure 4c. Although the gate dielectric was extremely thin, the gate leakage current was considerably low and stable. This improvement could be attributed to the uniform and pinhole-free deposition of the ultrathin Al_2O_3 gate dielectric film on the MoS_2 surface, facilitated by BCl_3 plasma-derived radical pretreatment. The distribution of electrical parameters for the top-gated FETs is plotted and compared with that for the pristine bottom-gated FETs in Figure S3. The average values of the extracted parameters for the top-gated FETs were as follows: on/off ratio of ~10^6, subthreshold swing of ~140 mV/dec, and field-effect mobility of ~9 $cm^2/(V\ s)$. These values indicate a reasonably high performance of the top-gated MoS_2-based FETs, which further highlights the potential of extending the technology to GAAFETs with a 2D channel material.

4. CONCLUSIONS

In conclusion, our study demonstrated the potential of the BCl_3 plasma-derived radical treatment as an effective 3D surface modification technique for MoS_2. This treatment improved the coverage and conformality of the ALD−Al_2O_3 films on both planar and suspended MoS_2 surfaces, demonstrating its applicability for future FETs with GAA structures. Our findings, supported by the OES, indicate that BCl_3 gas primarily decomposed into BCl radicals in the plasma state. Based on DFT calculations, the adsorption of these radicals on MoS_2 facilitated the chemical reactions with an Al precursor, enhancing the nucleation of ALD−Al_2O_3 films on MoS_2 surfaces. The reaction pathways determined through DFT calculations were experimentally verified through XPS analysis of the samples under different process conditions. Furthermore, a comparison of the Raman and PL spectra of monolayer MoS_2 and the electrical properties of bottom-gated bulk MoS_2 FETs before and after the BCl_3 plasma-derived radical treatment proved that the MoS_2 surface remained undamaged with some observed doping effects. Finally, the practicality of the treatment in terms of device performance was demonstrated through the electrical characterization of a top-gated bulk MoS_2 FET with an ultrathin ALD Al_2O_3 gate dielectric (~5 nm). This study provides valuable insights and experimental evidence for the application of BCl_3 plasma-derived radical treatment in the surface functionalization of MoS_2, thereby providing possibilities for the development of high-performance 3D-structured FET devices based on 2D materials.

■ ASSOCIATED CONTENT

Supporting Information

The Supporting Information is available free of charge at https://pubs.acs.org/doi/10.1021/acsami.3c09311.

> SEM images of ALD Al_2O_3 on MoS_2 with different process variables for BCl_3 plasma-derived radical treatment, fabrication process scheme of MoS_2 bridge sample, and statistical distribution of electrical parameters of bottom-gated and top-gated bulk MoS_2 FETs (PDF)

■ AUTHOR INFORMATION

Corresponding Authors

Geunyoung Yeom − *School of Advanced Materials Science and Engineering, Sungkyunkwan University, Suwon 16419, Republic of Korea*; orcid.org/0000-0002-1176-7448; Email: gyyeom@skku.edu

Hyoungsub Kim − *School of Advanced Materials Science and Engineering, Sungkyunkwan University, Suwon 16419, Republic of Korea*; orcid.org/0000-0003-3549-4250; Email: hsubkim@skku.edu

Authors

Heesoo Lee − *School of Advanced Materials Science and Engineering, Sungkyunkwan University, Suwon 16419, Republic of Korea*

Hoijoon Kim − *School of Advanced Materials Science and Engineering, Sungkyunkwan University, Suwon 16419, Republic of Korea*

Kihyun Kim − *School of Advanced Materials Science and Engineering, Sungkyunkwan University, Suwon 16419, Republic of Korea*

Kwangsik Jeong − *Division of Physics and Semiconductor Science, Dongguk University, Seoul 04620, Republic of Korea*; orcid.org/0000-0002-2804-7092

Mirine Leem − *School of Advanced Materials Science and Engineering, Sungkyunkwan University, Suwon 16419, Republic of Korea*

Seunghyun Park − *School of Advanced Materials Science and Engineering, Sungkyunkwan University, Suwon 16419, Republic of Korea*

Jieun Kang − *School of Advanced Materials Science and Engineering, Sungkyunkwan University, Suwon 16419, Republic of Korea*

Complete contact information is available at: https://pubs.acs.org/10.1021/acsami.3c09311

Author Contributions

[§]H.L., H.K., and K.K. made an equal contribution and are considered equal first authors.

Notes

The authors declare no competing financial interest.

■ ACKNOWLEDGMENTS

This work was supported by Samsung Electronics Co., Ltd (IO221021-03113-01), the GRRC Program of Gyeonggi Province (GRRC Sungkyunkwan 2023-B01), and the Next-generation Intelligence Semiconductor Program (2022M3F3A2A01072215) through the National Research Foundation of Korea (NRF) funded by the Ministry of Science and ICT.

■ REFERENCES

(1) Loubet, N.; Hook, T.; Montanini, P.; Yeung, C. W.; Kanakasabapathy, S.; Guillorn, M.; Yamashita, T.; Zhang, J.; Miao, X.; Wang, J.; Young, A.; Chao, R.; Kang, M.; Liu, Z.; Fan, S.; Hamieh, B.; Sieg, S.; Mignot, Y.; Xu, W.; Seo, S. C.; Yoo, J.; Mochizuki, S.; Sankarapandian, M.; Kwon, O.; Carr, A.; Greene, A.; Park, Y.; Frougier, J.; Galatage, R.; Bao, R.; Shearer, J.; Conti, R.; Song, H.; Lee, D.; Kong, D.; Xu, Y.; Arceo, A.; Bi, Z.; Xu, P.; Muthinti, R.; Li, J.; Wong, R.; Brown, D.; Oldiges, P.; Robinson, R.; Arnold, J.; Felix, N.; Skordas, S.; Gaudiello, J.; Standaert, T.; Jagannathan, H.; Corliss, D.; Na, M. H.; Knorr, A.; Wu, T.; Gupta, D.; Lian, S.; Divakarunni, R.; Gow, T.; Labelle, C.; Lee, S.; Paruchuri, V.; Bu, H.; Khare, M. Stacked

Nanosheet Gate-All-Around Transistor to Enable Scaling Beyond FinFET. *2017 Symposium on VLSI Technology*; IEEE, 2017; pp T230−T231.
(2) Das, U. K.; Bhattacharyya, T. K. Opportunities in Device Scaling for 3-nm Node and Beyond: FinFET versus GAA-FET versus UFET. *IEEE Trans. Electron Devices* **2020**, *67* (6), 2633−2638.
(3) Wang, Q. H.; Kalantar-Zadeh, K.; Kis, A.; Coleman, J. N.; Strano, M. S. Electronics and optoelectronics of two-dimensional transition metal dichalcogenides. *Nat. Nanotechnol.* **2012**, *7*, 699−712.
(4) Liu, Y.; Duan, X.; Huang, Y.; Duan, X. Two-Dimensional Transistors Beyond Graphene and TMDCs. *Chem. Soc. Rev.* **2018**, *47*, 6388−6409.
(5) Oviroh, P. O.; Akbarzadeh, R.; Pan, D.; Coetzee, R. A. M.; Jen, T. C. New Development of Atomic Layer Deposition: Processes, Methods and Applications. *Sci. Technol. Adv. Mater.* **2019**, *20* (1), 465−496.
(6) Hall, S.; Buiu, O.; Mitrovic, I. Z.; Lu, Y.; Davey, W. M. Review and Perspective of High-k Dielectrics on Silicon. *J. Telecommun. Inf. Technol.* **2007**, *2*, 33−43.
(7) Nam, T.; Seo, S.; Kim, H. Atomic Layer Deposition of a Uniform Thin Film on Two-Dimensional Transition Metal Dichalcogenides. *J. Vac. Sci. Technol., A* **2020**, *38*, 030803.
(8) Yang, J.; Kim, S.; Choi, W.; Park, S. H.; Jung, Y.; Cho, M. H.; Kim, H. Improved Growth Behavior of Atomic-Layer-Deposited High-k Dielectrics on Multilayer MoS_2 by Oxygen Plasma Pretreatment. *ACS Appl. Mater. Interfaces* **2013**, *5*, 4739−4744.
(9) Yang, W.; Sun, Q. Q.; Geng, Y.; Chen, L.; Zhou, P.; Ding, S. j.; Zhang, D. W. The Integration of Sub-10nm Gate Oxide on MoS_2 with Ultra Low Leakage and Enhanced Mobility. *Sci. Rep.* **2015**, *5*, 11921.
(10) Kim, S.; Choi, M. S.; Qu, D.; Ra, C. H.; Liu, X.; Kim, M.; Song, Y. J.; Yoo, W. J. Effects of Plasma Treatment on Surface Properties of Ultrathin Layered MoS_2. *2D Mater.* **2016**, *3*, 035002.
(11) Kim, K. H.; Kim, K. S.; Ji, Y. J.; Moon, I.; Heo, K.; Kang, D. H.; Kim, K. N.; Yoo, W. J.; Park, J. H.; Yeom, G. Y. Effect of Large Work Function Modulation of MoS_2 by Controllable Chlorine Doping using a Remote Plasma. *J. Mater. Chem. C* **2020**, *8*, 1846−1851.
(12) Kim, H. High-k Dielectric Integration on MoS_2 for Next Generation Electronic Devices. Ph. D. Dissertation, Sungkyunkwan University, 2022.
(13) Liu, H.; Xu, K.; Zhang, X.; Ye, P. D. The Integration of High-k Dielectric on Two-Dimensional Crystals by Atomic Layer Deposition. *Appl. Phys. Lett.* **2012**, *100*, 152115.
(14) Matero, R.; Rahtu, A.; Ritala, M.; Leskelä, M.; Sajavaara, T. Effect of water dose on the atomic layer deposition rate of oxide thin films. *Thin Solid Films* **2000**, *368*, 1−7.
(15) Kresse, G.; Joubert, D. From Ultrasoft Pseudopotentials to the Projector Augmented-Wave Method. *Phys. Rev. B: Condens. Matter Mater. Phys.* **1999**, *59*, 1758−1775.
(16) Kresse, G.; Furthmüller, J. Efficiency of Ab-Initio Total Energy Calculations for Metals and Semiconductors using a Plane-Wave Basis Set. *Comput. Mater. Sci.* **1996**, *6* (1), 15−50.
(17) Perdew, J. P.; Ruzsinszky, A.; Csonka, G. I.; Vydrov, O. A.; Scuseria, G. E.; Constantin, L. A.; Zhou, X.; Burke, K. Restoring the Density-Gradient Expansion for Exchange in Solids and Surfaces. *Phys. Rev. Lett.* **2008**, *100* (13), 136406.
(18) Jackson, S. T.; Nuzzo, R. G. Determining Hybridization Differences for Amorphous Carbon from the XPS C 1s Envelope. *Appl. Surf. Sci.* **1995**, *90*, 195−203.
(19) Desai, S. B.; Madhvapathy, S. R.; Amani, M.; Kiriya, D.; Hettick, M.; Tosun, M.; Zhou, Y.; Dubey, M.; Ager, J. W.; Chrzan, D.; et al. Gold-Mediated Exfoliation of Ultralarge Optoelectronically-Perfect Monolayers. *Adv. Mater.* **2016**, *28*, 4053−4058.
(20) Lee, C.; Yan, H.; Brus, L. E.; Heinz, T. F.; Hone, J.; Ryu, S. Anomalous Lattice Vibrations of Single- and Few-Layer MoS_2. *ACS Nano* **2010**, *4* (5), 2695−2700.
(21) Mouri, S.; Miyauchi, Y.; Matsuda, K. Tunable Photoluminescence of Monolayer MoS_2 via Chemical Doping. *Nano Lett.* **2013**, *13* (12), 5944−5948.
(22) Ahn, J. H.; Parkin, W. M.; Naylor, C. H.; Johnson, A. T. C.; Drndić, M. Ambient Effects on Electrical Characteristics of CVD-Grown Monolayer MoS_2 Field-Effect Transistors. *Sci. Rep.* **2017**, *7*, 4075.

https://doi.org/10.1021/acsami.3c09311
ACS Appl. Mater. Interfaces 2023, 15, 46513−46519